Defective Fuel Examination Using Coulometric Titration and Analytical Electron Microscopy at Chalk River Laboratories

Z. He[a], J. Mouris[b], R. Ham-Su[c]

Abstract. Although the fuel failure rate is very low in CANDU reactors, hot cell examination and characterization of representative defected fuels are performed on a continuing basis within fuel surveillance programs. The objectives are to fully understand defective fuel behavior during irradiation and to further develop fuel behaviour models. This paper describes some techniques used at Chalk River Laboratories (CRL) for quantitative oxygen measurements on representative pellets from defected fuels, which were oxidized due to coolant ingress into the fuels during irradiation. When needed, quantitative O/M (i.e., oxygen to metal atom) ratio measurements are performed using a coulometric titration technique developed at CRL. This technique can determine the O/M ratio of fuel pellet samples taken by core drilling from an irradiated pellet. Further, electron probe analysis may be carried out using a shielded scanning electronic microscope to determine the extent of local oxidation in a fuel pellet. X ray wavelength dispersive spectrometry is used to determine the local oxygen and uranium concentration, thereby determining the local O/U ratio. The analysis can be performed in a very local region (e.g., close to a through-wall sheath defect) owing to its spatial resolution of 2–3 microns. By using these techniques, and with known irradiation histories for defective fuel elements, detailed information required for fuel behavior modeling is obtained.

1. INTRODUCTION

The change in oxidation state of UO_2 during irradiation alters its thermal conductivity, melting point and diffusion controlled processes such as fission gas release, creep and grain growth [1–3]. Quantitative knowledge of the oxidation state of irradiated fuel can provide significant insight into fuel structure and behaviour and aid the development of fuel performance models. Oxygen distribution varies within pellets inside a defected fuel element during irradiation [1–5]; however, detailed knowledge of its distribution is limited.

Although the defect rate of CANDU fuel is low, post irradiation examination (PIE) of defective fuel elements is conducted at AECL Chalk River Laboratories (CRL) on a continuing basis within fuel surveillance programs. This ensures safe operation of CANDU fuels and facilitates further development of computer codes to simulate in-core defected fuel behaviour. Characterization of oxygen distribution in defected fuel has been ongoing at CRL for a number of years [6–7]. As a macroscopic analytical tool (millimetre scale), the coulometric titration (CT) technique developed at CRL provides a general picture with respect to the extent of pellet oxidation inside a defective fuel element.

[a] Fuel Development Branch, AECL Chalk River Laboratories, Canada
[b] Fuel Development Branch, AECL Chalk River Laboratories, Canada
[c] Fuel Development Branch, AECL Chalk River Laboratories, Canada

Using optical microscopy, scanning electron microscopy (SEM) and electron micro probe analysis (EPMA), pellet oxidation can be further characterized (micro meter scale) and related information (for example, the associated grain growth and condition of fission gas release) can be revealed. With the combination of these macro- and micro-analytical techniques, the oxidation condition of a defective fuel element can be systematically quantified and the results can be used to develop defective fuel models [3].

This paper primarily focuses on describing techniques used at CRL for characterization of UO_2 pellet specimens from defective fuel elements. Results of these characterizations are also provided.

2. COULOMETRIC TITRATION TECHNIQUE

2.1. Working principle

Fig. 2.1 is a schematic diagram of the CT apparatus. Ar gas containing 2000 ppm H_2 is passed over the sample in the furnace at room temperature – no reaction between the sample and gas occurs. Downstream, the gas is passed through the ceramic CT cell, which measures the quantity of oxygen (O/M ratio) required to convert all the H_2 to H_2O (further described in the next paragraph). Next, the sample in the furnace is heated to 1000°C, nominally at a heating rate of 5°C per minute. When the temperature is sufficiently high, the gas and sample begin to react. Consequently, the H_2 in the gas flow converts UO_{2+x} to stoichiometric UO_2. Because the temperature only rises to 1000°C, the sample cannot become substoichiometric. This process continues until no further oxygen is released from the sample, rendering it stoichiometric. The decrease in the amount of H_2 in the gas, delivered to the downstream CT cell, is integrated; thereby, the amount of oxygen being released from the sample, x, is calculated.

A schematic diagram of the ceramic CT cell is shown in Fig. 2.2. The gas flows through a tube composed of zirconia (ZrO_2) doped with 8 mol% yttria (Y_2O_3). During operation, the CT cell is maintained at 750°C. At this temperature, this material readily conducts oxygen ions through the lattice, but will not conduct free electrons as metals do. Thus, when an electrical voltage is applied, oxygen ions are free to move, but free electrons are not. Therefore, any electrical current measured is an indication of oxygen ion transport. At the gas inlet, a voltage is created through the tube wall and current flows, in the form of oxygen ions. The air surrounding the tube allows oxygen ions to form at the outer surface of the tube. They pass through the wall where they recombine with other oxygen ions at the inner surface and desorb from the cell surface as O_2 (or combine directly with the H_2 in the gas to form H_2O). In this way, O_2 is passed from atmospheric air through the cell wall to the gas stream in the CT tube. At the CT gas-outlet, the voltage between the inner surface and outer surface is measured. This voltage can be used to directly measure the O_2 partial pressure in the tube relative to the O_2 partial pressure in the air atmosphere. A feedback loop from this voltage controls the oxygen current inflow at the inlet end of the tube. In this way, only enough O_2 is provided to convert all H_2 to H_2O. (In fact, the O_2 content in the tube is always brought to a small fixed quantity of O_2 – about 40 ppm – this ensures that the H_2 quantity is extremely low).

To verify and calibrate the CT equipment, U_3O_8 is used to measure the change in stoichiometry to convert it to UO_2. The error in these tests is required to be below 1% of the change in O/U ratio. For UO_{2+x} samples with lower O/U ratios – about 2.10 – the uncertainty is about 5% of the change in stoichiometry (i.e., 0.005). Another source of uncertainty results from grinding the fuel samples into fine particles where some oxidation of the powder occurs prior to CT measurement. This can lead to an uncertainty of 0.01 in the stoichiometry change. For dense, non-friable fuel samples, this is the major source of error.

Fig. 2.3 shows the result of an O/M-ratio measurement of an irradiated fuel sample from a fuel element with a through-wall sheath defect. The *titration current* represents the amount of oxygen ions required in the CT cell to exactly convert all H_2 to H_2O. Assuming that all oxygen released from the

sample during the measurement came from altering the stoichiometry of the UO_2 (not from other phases that may have been present), the fuel sample is determined to have had an initial stoichiometry of $UO_{2.072}$ in this case. However, this is an upper limit because other phases in the fuel sample (e.g., oxidized fission-product phases) might also have released oxygen. Due to the low burn-up of this fuel, the amount of the other oxidized phases is expected to be small.

2.2. Sample preparation for CT measurement

In a hot cell, 50–200 mg fuel samples were obtained from specific radial and longitudinal pellet-stack locations in an irradiated fuel element with a through-wall sheath defect. This was accomplished by cutting approximately 10 mm pellet sections from the element and drilling them at precise positions with a 1.8 mm diamond drill, parallel to the element axis. Samples were then loaded into a glove box and placed in the CT furnace.

2.3. Example of CT results

Fig. 2.4 shows how the extent of pellet oxidation inside a defected fuel element is quantified. As shown, all samples exhibited oxidation; the O/M values varied from 2.02–2.10. The centre cross-section (Section 6) exhibited slightly lower O/M values than the end-sections because sheath defects occurred at both ends of the fuel element.

Ceramographic analysis indicated the presence of higher oxide phases and enhanced grain growth in the element, as described below.

Primary defect:
The primary defect, caused by fretting damage, was small and no UO_2 loss was observed. UO_2 oxidation was observed along the exterior of the pellet and at a major radial crack (Fig. 2.5). Also, the grain boundaries in this vicinity were oxidized (Fig. 2.6). Moreover, at the centre of this region, the grain size was about 17 μm, compared with 6 μm at the periphery (the as-manufactured grain size was 6 μm). This, and the observed intergranular gas bubbles and tunnels are unexpected at this power (29 $kW \cdot m^{-1}$) and burn-up (3.4 $MW \cdot d \cdot kg^{-1}$ U) for intact fuel elements. Their presence is consistent with the observed pellet oxidation in this region, since pellet oxidation reduces thermal conductivity (increasing temperature), thereby enhancing UO_2 grain growth and fission-gas release [1].

Secondary defect:
The secondary defect of the element was relatively large (about 13 mm^2, see Fig. 2.7) and UO_2 loss near the defect was observed.

In the mid-radius of this region, fuel oxidation was observed at cracks (Fig. 2.8). Islands of grains appeared throughout the oxidation phase, indicating preferential grain boundary oxidation. In the central region (not shown), oxidation along radial cracks was also observed, but the extent of oxidation was not as great as that in the mid-radius region.

Besides oxidation, UO_2 grain growth was observed in the mid-radius (14 μm; Fig. 2.9), and the central regions (30 μm) – the as-fabricated grain size was 6 μm. Gas bubbles and tunnels were observed at the grain boundaries in both regions. These observations are indicative of decreased thermal conductivity.

3. SEM/WDS QUANTIFICATION OF FUEL PELLET OXIDATION

3.1. Wavelength dispersive X-ray spectroscopy (WDS)

X-rays emitted from a specimen bombarded with a focused electron beam in a scanning electron microscope (SEM) can be used to identify which elements are present (qualitative analysis). With an optimized experimental set up and data-analysis procedures, the measured X-rays can also be used to

quantitatively evaluate the chemical composition of the sample.

WDS is an electron probe micro-analytical (EPMA) technique with a spatial resolution of the order of 10 μm^3, and high spectral resolution of the order of 10 eV [8]. It detects elemental constituents in a surface layer of about 1–2 microns [9]. Quantitative WDS analysis is performed in relation to a known standard. If the standard is of composition, structure and density similar to the sample analysed, its fractional amount in the unknown with respect to the standard is given by:

$$\frac{C}{C_o} = \frac{I}{I_o} \tag{1}$$

Where C and C_o are the weight percentages of the probed element in the sample and the standard, I and I_o, are the peak intensities measured in the sample and the standard.

WDS requires the selection of a characteristic X-ray wavelength from the element analyzed. The X-rays from the sample are selected by wavelength using diffracting crystals. Different types of crystals are used depending on the wavelength to be analyzed and each crystal may detect only one element. As a consequence, WDS analysis is highly accurate but relatively time consuming.

3.2. Specimen preparation

An irradiated fuel pellet sample from a defected element and a sample of unirradiated UO_2 (to be used as a standard) were positioned together in a conductive metallographic mount. The metallographic sample was ground to 600 grit using SiC paper. This was followed by a two-stage polish, first with aqueous 0.05 μm Al_2O_3 suspension and secondly with colloidal silica (average particle size of 40 nm). The sample was then slightly etched with a solution of H_2O_2/H_2SO_4 ((90/10)%) to reveal the grain boundaries. The sample was re-polished and lightly etched using the same process in preparation for the present work. A secondary electron image of the overall sample is shown in Fig. 3.1. For analysis, the sample was divided into four regions: centre, mid-radius, periphery and edge.

3.3. SEM and WDS analysis

Analytical scanning electron microscopy (SEM) was performed using a radiation shielded instrument. secondary electron images (SEI) of the sample surface were taken at an acceleration voltage of 25 kV.

The WDS system used was equipped with Geller MicroAnalytical dQant software. The acceleration voltage applied for this study was 20 kV, which was recommended by the manufacturer for oxygen analysis. Two crystals were utilized during the analysis: pentaerythritol, to detect uranium (Mα peak, wavelength = 0.391 nm) and a synthetic layered dispersive element for oxygen (Kα peak, wavelength = 2.362 nm). An example of the uranium and oxygen peaks is given in Fig. 3.2.

Four different locations were measured in the sample (Table 3.1).

TABLE 3.1 FOUR DIFFERENT MEASUREMENT LOCATIONS

Central region	$r/r_o = 0$
Mid-radius	$r/r_o = 0.5$
Periphery	$r/r_o = 0.8$
Edge	$r/r_o = 1$

For each location, point analysis along a line close to the tangential direction was performed. Each analysis set was composed of 30–60 points and each point was measured 5 times, for 30 seconds. Each point-intensity, I, was calculated from the average of the five (30-second) readings:

$$I_{oxygen} = \frac{\sum_5 I_{sample.oxygen}}{5} \tag{2}$$

$$I_{uranium} = \frac{\sum_5 I_{sample.uranium}}{5} \tag{3}$$

WDS analysis requires a reference-intensity value for quantitative analysis. The results presented here used the average of 11 standard readings to calculate an average reference intensity I_o:

$$I_{o-oxygen} = \frac{\sum_{11} I_{std.oxygen}}{11} \tag{4}$$

$$I_{o-uranium} = \frac{\sum_{11} I_{std.uranium}}{11} \tag{5}$$

The intensities measured in the sample were then normalized with respect to the standard:

$$I_{norm} = \frac{I}{I_o} \tag{6}$$

3.3.1. WDS point analysis along a line

A micrograph of the central area where WDS was performed is shown in Fig. 3.3. The yellow line indicates the site of the analyses. The spacing between the points forming the analysis line was 5 μm for the centre and mid-radius regions, and 3 μm for the periphery and the edge regions. The SEM image of Fig. 3.3 shows that the sample surface is not featureless. There are fine cracks observable on the surface; lenticular pores and dimples are visible (likely the result of the creation of fission gas); line scratches resulting from the initial stages of ceramographic preparation, are also evident. These features will have an effect on the WDS analysis results. For example, the presence of voids and microcracks will result in lower U and O peak intensities.

The normalized (with respect to the standard) oxygen and uranium intensities (as a function of position for the central region line scan) are shown in Fig. 3.4. The uncertainty associated with each point is expressed as the standard deviation (σ) attained and shown through the error bars. Variations in intensity occur in both the uranium and oxygen peaks. For the most part, the variation is small and peak intensities are relatively uniform within each region. Nevertheless, relatively large intensity variations can be observed sporadically in the graphs, as in the first 15 μm of the central region line scan (Fig. 3.4).

The WDS results showed that oxygen and uranium peak intensities are consistent from grain to grain within a region. In general, the large variations in intensity observed can be attributed to microstructural features such as pores and grain boundaries.

Ideally, the variations in intensity between sample and standard are only due to differences in composition. The underlying assumption, in Equations 1, 6 and the WDS analysis performed so far, is that the measured X-ray intensity difference between sample and standard is due to their basic compositional difference.

In some cases, the intensity variations cannot be easily correlated with height variations on the surface. For example, the first three points measured in the central region (Fig. 3.4) show a decreased intensity. In the absence of topographical features, these variations are a result of the presence of microvoids, or other elements and compounds. The data analysis software calculates the percentage of uranium and

oxygen in a spot (using the standard as a reference). If the percentage of uranium added to the percentage of oxygen is not approximately 100%, this is a strong indication of the presence of microvoids or other elements in the spot analyzed. Hence, for further data analysis, the points acquired where the sum of the oxygen and uranium percentages was not close to 100% were removed.

Oxygen and Uranium Distribution

The average oxygen and uranium normalized intensities as a function of radial position are shown in Fig. 3.4. The amount of oxygen increases towards the edge. However, the oxygen intensities can be normalized with respect to the uranium intensities to attain a relative O/U concentration ratio. Calculated this way, the UO_2 standard would have an O/U concentration ratio of 1. The results and their uncertainty, calculated from the standard deviations, are shown in Fig. 3.6. These results indicate an increased O/U concentration ratio in the mid-radius, which agrees with previous CT measurements and modeling predictions [3]. The cause of the irregular uranium distribution shown in Fig. 3.5 (i.e., lower uranium intensity readings in the central and mid-radius regions) is uncertain, but likely related to temperature- and irradiation-dependent changes in pellet structure and density occurring during operation.

From the results shown in Fig. 3.5, the U content in the irradiated fuel sample is lower than in the standard. This is expected due to fissioning of U. In addition, microstructural/density changes (e.g., creation of fission-gas bubbles) will also affect the intensity of the U X-ray signal. Separating these effects may be possible by analyzing a non-defected fuel where only temperature and radiation effects are present. The structural and density changes that occur during operation may then be discerned from the oxidation related to the presence of defects.

Standard

In this work, an unirradiated UO_2 pellet was used as the standard; however, as mentioned previously, structural changes that occurred in the sample may affect the interaction and absorption of X-rays. Therefore, the assumption that the standard and sample are essentially equal except for composition (Equations 1 and 6) may not be exactly valid. It is being considered to use a non-defected fuel with similar burn-up as a standard. This will enable a relative measure of oxidation in the defected fuel.

4. SUMMARY

Characterization of oxygen distribution at macro- and microscopic levels in defected fuel has been ongoing at CRL for a number of years. The CT technique provides a macroscopic measurement of the extent of pellet oxidation inside a defective fuel element. Pellet oxidation can be further characterized using optical microscopy, SEM and EPMA techniques. With the combination of these macro- and micro-analytical techniques, the oxidation condition of a defective fuel element can be systematically quantified, and the information and data can be used to develop defective fuel models. The work described in this paper demonstrates that CT-based O/M measurements, optical microscopy and SEM/WDS analyses produce converging results.

The accuracy of WDS measurements is expected to be improved by taking the following precautions:

a) The specimen should be polished in such a way that it is as flat and scratch-free as possible.
b) Using diamond-based, water-soluble polishing pastes will reduce oxygen, aluminum and silicon contamination in cracks and crevices.
c) Using an irradiated pellet from an intact fuel element as a standard (with similar burn-up to the sample) will facilitate the relative measure of oxidation in the defected fuel.

5. ACKNOWLEDGEMENTS

The authors would like to thank Craig Buchanan and Pam Ryan at CRL for optical examination and SEM/WDS analyses, respectively.

The work reported in this paper was funded by the CANDU Owners Group R&D, Safety and Licensing Program**,** under the joint participation of Atomic Energy of Canada Limited, Hydro-Québec, New Brunswick Power Nuclear, Ontario Power Generation, Bruce Power, and Societatea Nationala Nuclearelectrica (Romania).

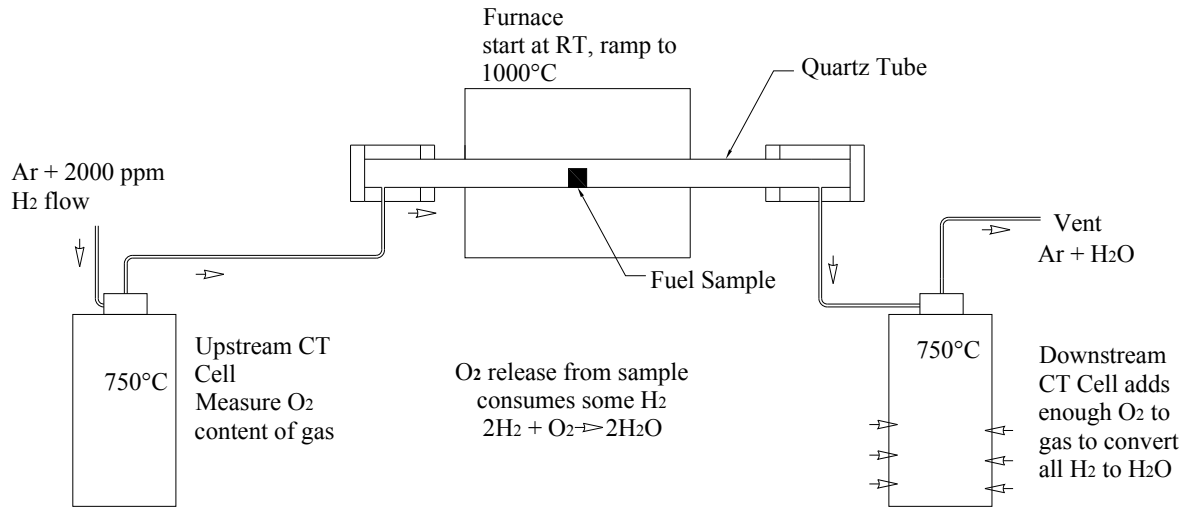

FIG 2.1. Schematic diagram of coulometric titration apparatus.

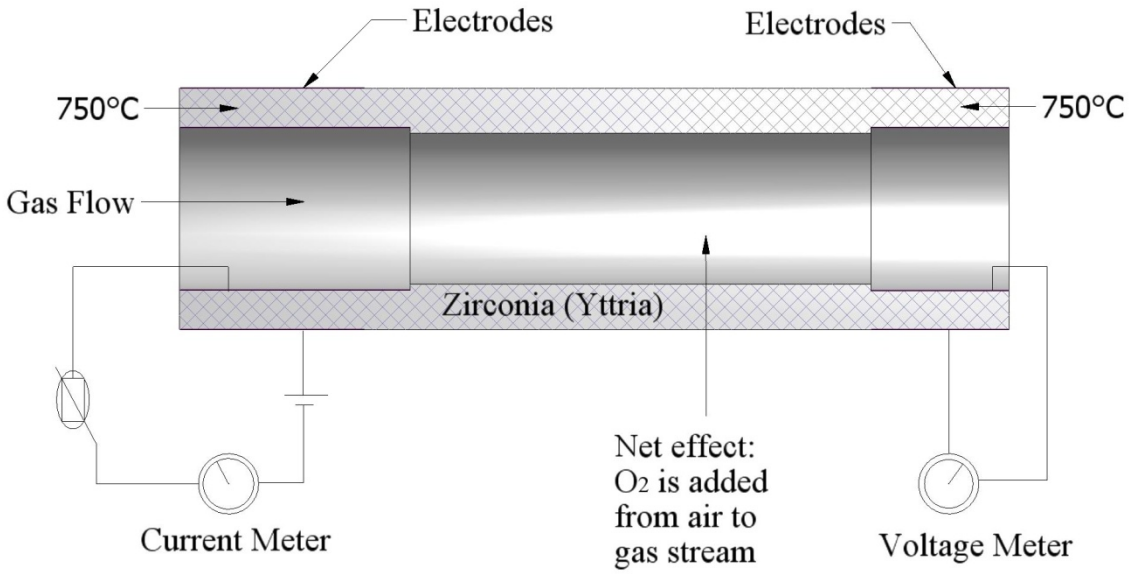

FIG. 2.2. Rough schematic diagram of a CT cell. Doping ZrO_2 with Y_2O_3 increases the O^{2-} vacancy concentration, thus enhancing the O^{2-} diffusion rate. Measuring the electric current (I) gives the O^{2-} diffusion rate. Measuring the voltage (U) gives the O_2 partial pressure inside the tube relative to the value outside the tube.

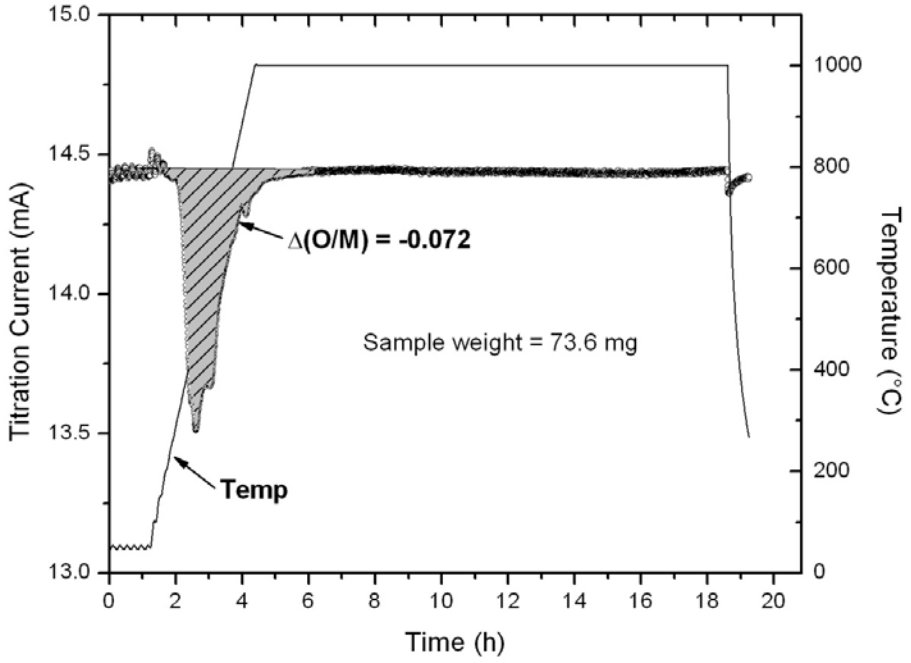

FIG. 2.3. Reduction of an irradiated sample of fuel with a through-wall clad-defect.

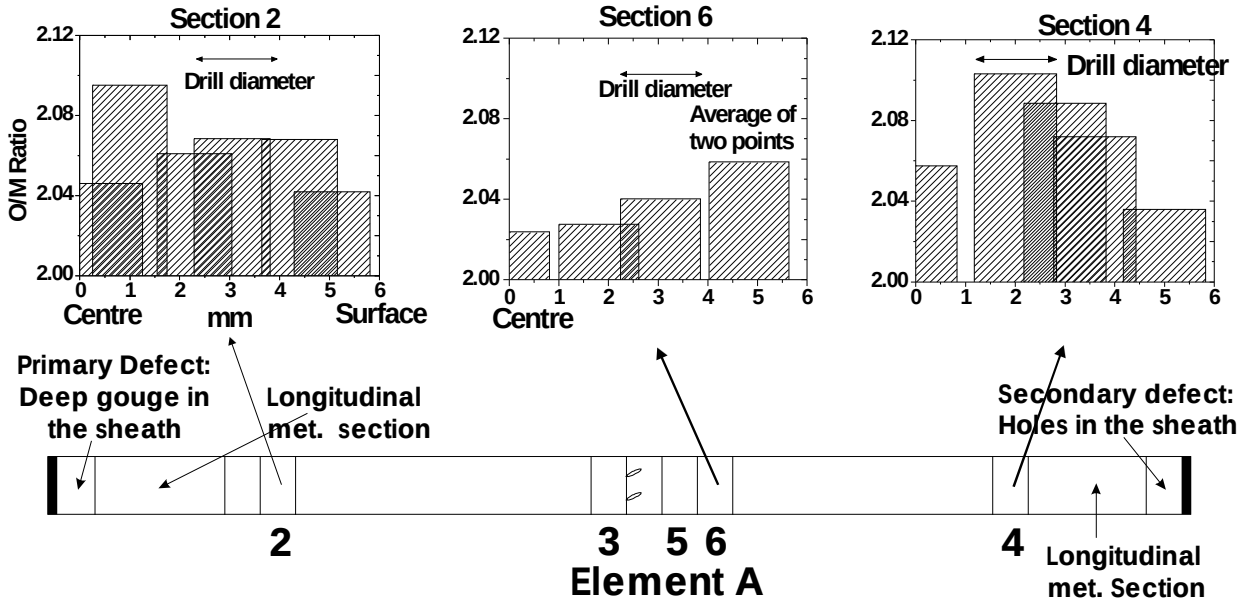

FIG. 2.4. O/M measurements on a defective fuel element.

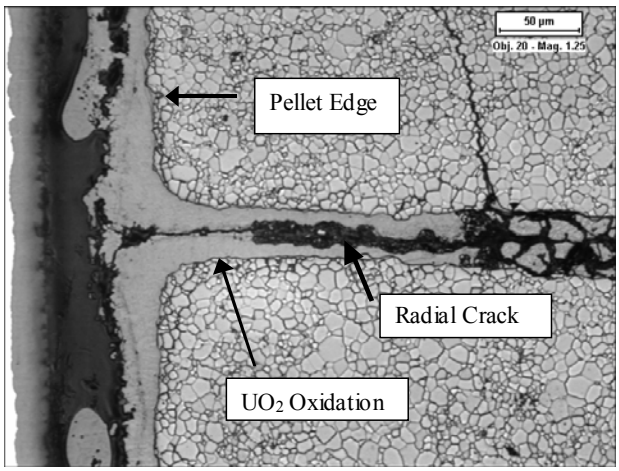

FIG. 2.5. Primary (fretting) defect – showing fuel oxidation on the pellet edge and radial crack.

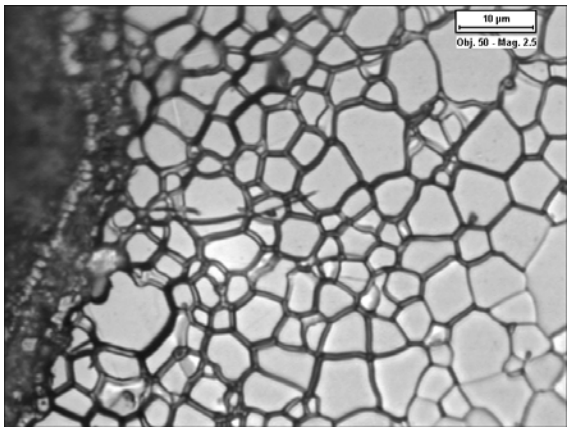

FIG. 2.6. Primary (fretting) defect – higher magnification than Fig. 3.5, showing fuel grain boundary oxidation near a radial crack.

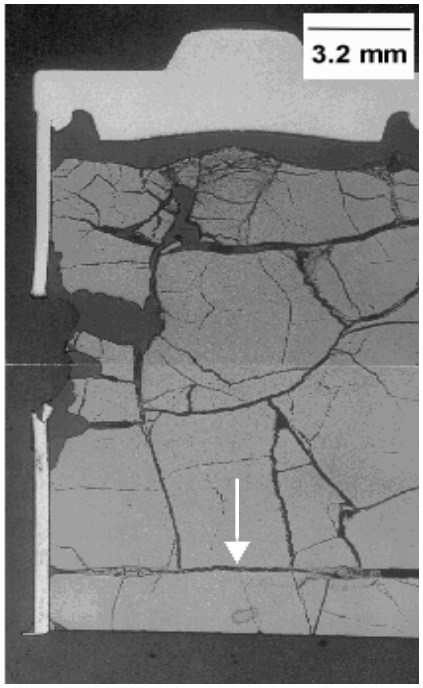

FIG. 2.7. At the secondary defect (a hole), low magnification – shows fuel local loss from hole, cracks and pellet-pellet interface (arrow).

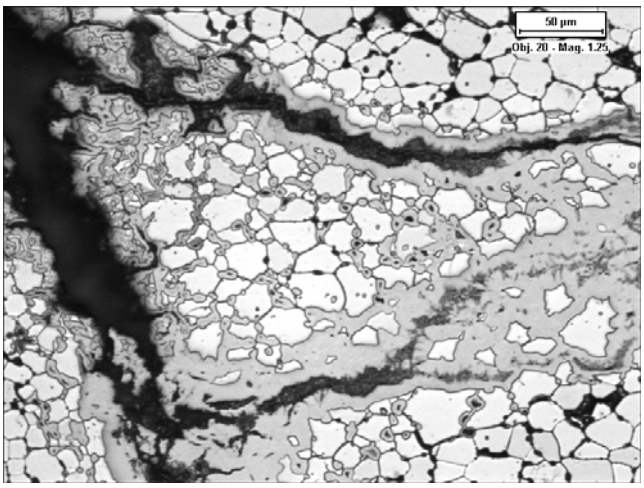

FIG. 2.8. At secondary defect mid-radius (i.e., 3.5 mm from the centre) along a radial crack – shows isolated grains embedded in darker fuel oxidation.

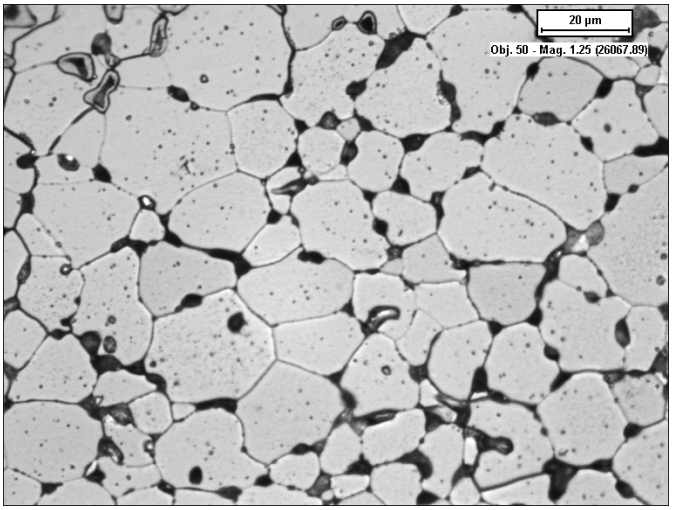

FIG. 2.9. At secondary defect mid-radius (i.e., 3 mm from centre) – shows grain growth (average grain size 14 µm), and fission gas bubbles in grain boundaries and tunnels.

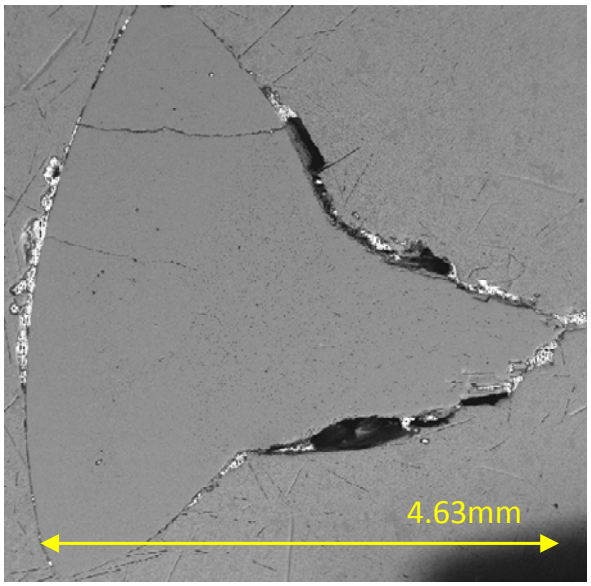

FIG. 3.1. Secondary electron image (SEI) of the pellet sample.

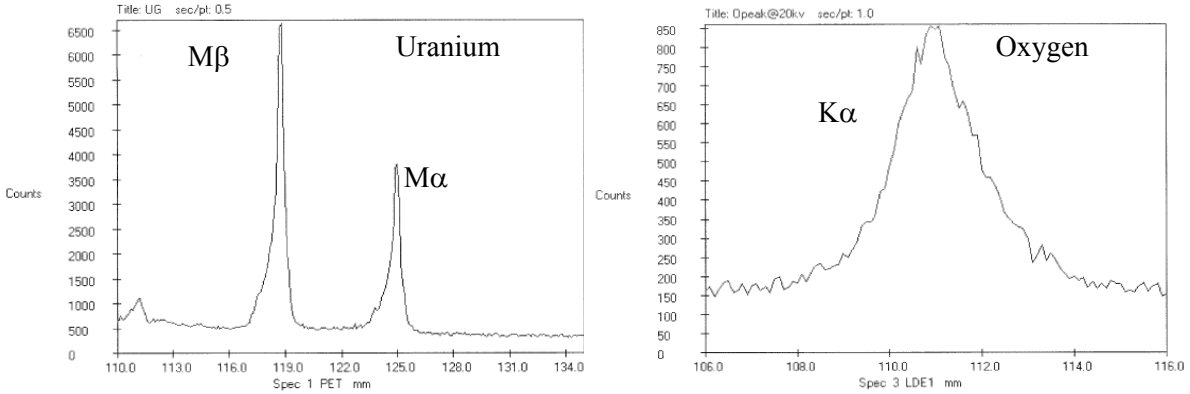

FIG. 3.2. WDS uranium and oxygen peaks at 20 kV; Note: The horizontal axis indicates the distance from the X-ray source to the analyzing crystal.

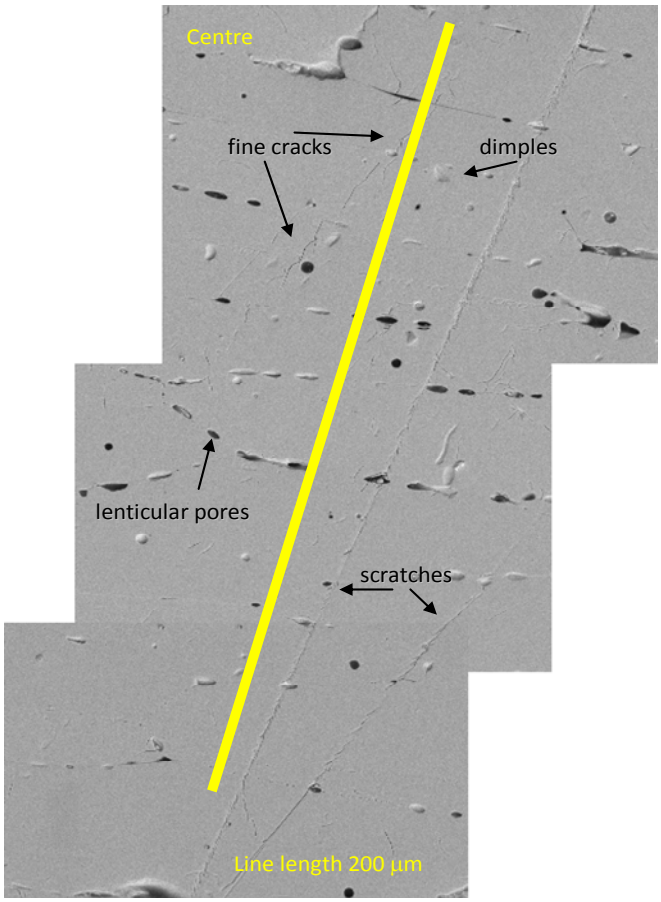

FIG. 3.3. WDS: central region.

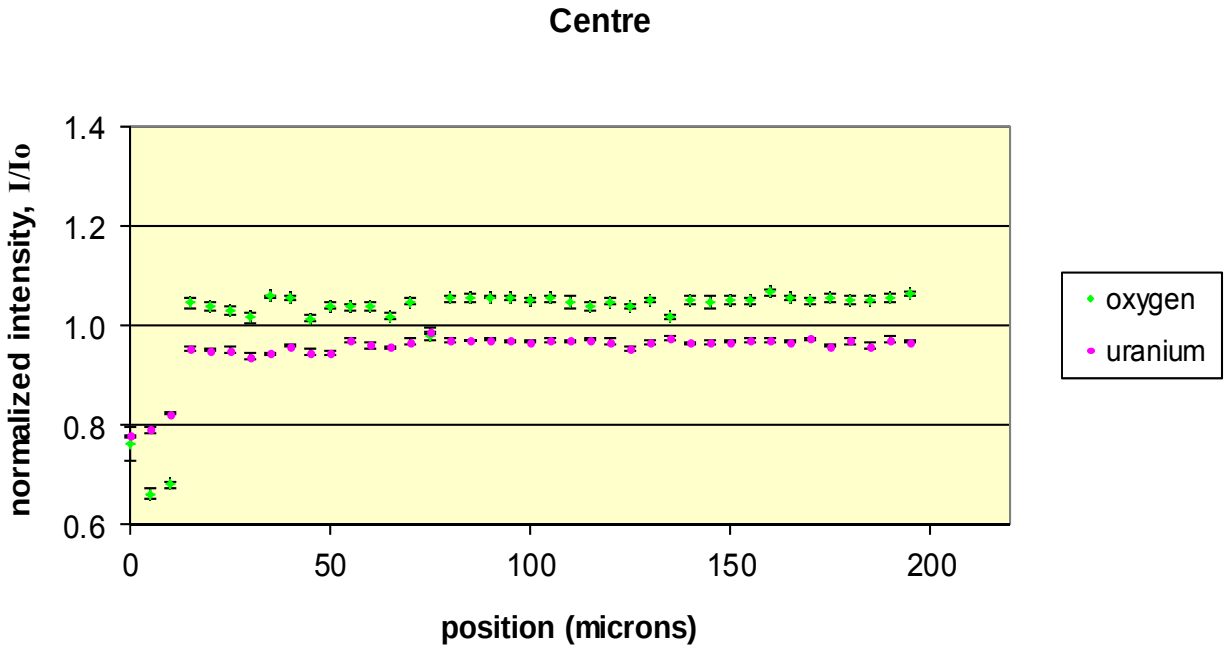

FIG. 3.4. Normalized oxygen and uranium intensities: central region; the error bars indicate the precision (σ) of the measurements.

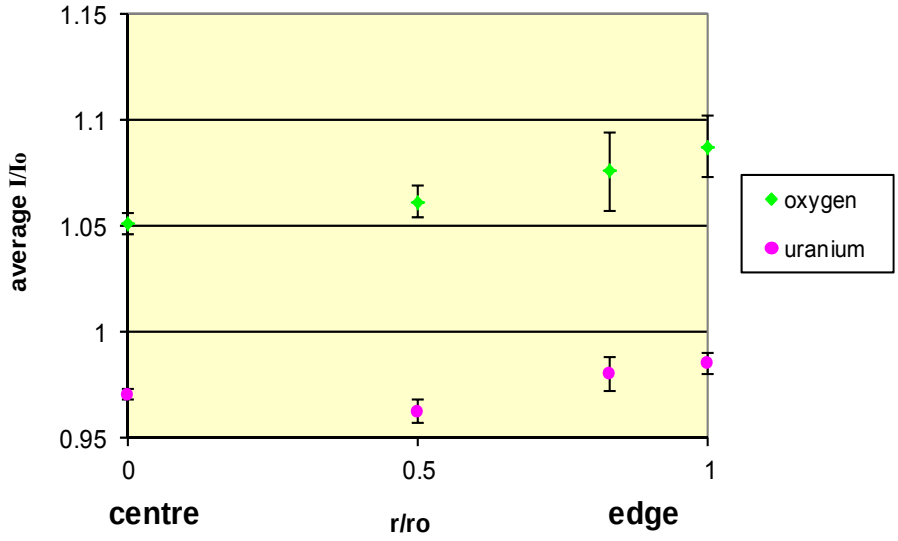

FIG. 3.5. Average oxygen and uranium normalized intensities (error bars denote the standard deviation of each point).

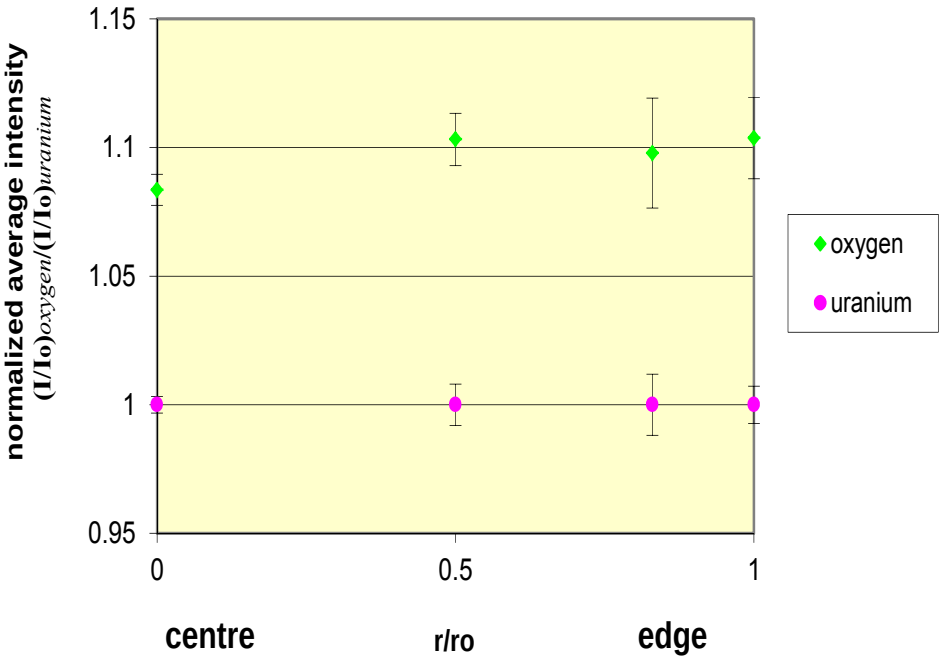

FIG. 3.6. normalized intensities with respect to uranium intensity (error bars denote the calculated uncertainty).

REFERENCES

[1] WALKER, C.T., RONDINELLA, V.Z.V., PAIOANNOU, D., VAN WINCKEL, S., GOLL, W., MANZEL, R., On the oxidation state of UO_2 nuclear fuel at a burn-up of around 100 MWd/kgHM, Journal of Nuclear Materials **345** (2005) 192–205.

[2] VERRALL, R.A., MOURIS, J.F., O/M ratio measurement techniques, 8th International Conference on CANDU Fuel (2003) 65–73.

[3] HIGGS, J., LEWIS, B.J., THOMPSON, W.T., HE, Z., A conceptual model for the fuel oxidation of defective fuel, Journal of Nuclear Materials **366** (2007) 99–128.

[4] LEWIS, B.J., IGLESIAS, F.C., COX, D.S., GHEORGHIU, E., A model for fission gas release and fuel oxidation behaviour for defected UO_2 fuel elements, Nuclear Technology **92** (1990) 353–362.

[5] LEWIS, B.J., MACDONALD, R.D., IVANOFF, N.V., IGLESIAS, F.C., Fuel performance and fission product release studies for defected fuel elements, Nuclear Technology **103** (1993) 220–245.

[6] VERRALL, R.A., HE, Z., MOURIS, J.F., Characterization of fuel oxidation in rods with clad-holes, Journal of Nuclear Materials **344** (2005) 240–245.

[7] HAM-SU, R., HE, Z., RYAN, P., Wavelength dispersive X-ray spectroscopy (WDS) on defected fuel, Proceedings of the 10th CNS International Conference on CANDU Fuel (2008).

[8] BARKER, W., FOURNELLE, J., X-ray compositional microanalysis, Department of Geology and Geophysics, University of Wisconsin-Madison (1995).

[9] GOLDSTEIN, I., NEWBURY, D.E., ECHLIN, P., JOY, D.C., ROMIG, Jr. A.D., LYMAN, C.E., FIORI, C., LIFSHIN, E., Scanning electron microscopy and X-ray microanalysis, Second Edition, Plenum Press, New York (1992).

[10] EXNER, H.E., WEINBRUCH, S., Scanning electron microscopy, Metallography and Microstructures, Vol. 9, ASM Handbook, ASM International (2004) 355–367.

[11] ASTM INTERNATIONAL, Standard test methods for determining average grain size, ASTM E112-96 (1996).